Magnetic Resonance in Medicine 46:272–281 (2001)

Quantification of the Effect of Water Exchange in Dynamic Contrast MRI Perfusion Measurements in the Brain and Heart

Henrik B.W. Larsson,* Sverre Rosenbaum, and Thomas Fritz-Hansen

Measurement of myocardial and brain perfusion when using exogenous contrast agents (CAs) such as gadolinium-DTPA (Gd-DTPA) and MRI is affected by the diffusion of water between compartments. This water exchange may have an impact on signal enhancement, or, equivalently, on the longitudinal relaxation rate, and could therefore cause a systematic error in the calculation of perfusion (*F*) or the perfusion-related parameter, the unidirectional influx constant over the capillary membranes (K_i). The aim of this study was to quantify the effect of water exchange on estimated perfusion (*F* or K_i) by using a realistic simulation. These results were verified by in vivo studies of the heart and brain in humans. The conclusion is that water exchange between the vascular and extravascular extracellular space has no effect on K_i estimation in the myocardium when a normal dose of Gd-DTPA is used. Water exchange can have a significant effect on perfusion estimation (*F*) in the brain when using Gd-DTPA, where it acts as an intravascular contrast agent. Magn Reson Med 46:272–281, 2001. © 2001 Wiley-Liss, Inc.

Key words: contrast-enhanced MRI; water residence time; myocardial perfusion; brain perfusion

Measurement of perfusion when using exogenous contrast agents (CAs) and MRI is affected by the diffusion of water between compartments. Several studies have indicated that this could affect the results of such perfusion measurements (1–6). However, contrast-enhanced MRI using T_1-weighted imaging has been developed in order to measure perfusion or perfusion-related parameters of the heart in vivo without explicitly considering the effect of water exchange. Models of perfusion in animals and humans when using extravascular CAs such as gadolinium-DTPA (Gd-DTPA) or intravascular CA have been presented (7–12). These measurements are often based on inversion recovery turboFLASH (IR-turboFLASH) or saturation recovery turboFLASH (SAT-turboFLASH) imaging.

Most of these studies measure the tissue enhancement curve and the arterial input function and rely on basic tracer kinetic models as formulated by Kety (13). In the ideal case, this approach gives the unidirectional influx constant K_i (ml/100 g/min) for CA diffusion over the capillary membrane when extravascular CA is used and the perfusion F (ml/100 g/min) when intravascular CA is used. For extravascular CA, the perfusion and the unidirectional influx constant are related by $K_i = EF$ (14), where E is the unidirectional extraction fraction in the first pass.

There is now growing evidence that K_i in particular provides valuable and clinically useful information related to perfusion (7–12,15). For example, it has been shown previously that infusion of dipyridamole in humans resulted in an increase of K_i by a factor of 2–3 in the heart of healthy subjects. In patients with ischemic heart disease, K_i was either unaffected or decreased after infusion of dipyridamole in areas supplied by an insufficient coronary artery (16,17).

Many assumptions need to be investigated in order to clearly associate directly the MRI-determined K_i with the physiological parameter, the unidirectional influx constant of the CA diffusion over the capillary membrane in the heart. One of the main concerns is related to the fact that CA is measured indirectly through water relaxation. Water diffuses between compartments and this exchange of water between compartments can modify the MR signal enhancement of the tissue (1) and, therefore, influence the measured K_i. Hence, water exchange can potentially affect the results obtained with both extravascular and intravascular CA.

This study investigates quantitatively the effect of water exchange between intravascular and extravascular compartments and focuses on the effect on K_i when using an extravascular CA and the effect on perfusion (F) when using an intravascular CA. The effect of water exchange was quantified by computer simulations. First, a simple approach was used by simulating two extreme situations: the fast water exchange regime, defined as $1/\tau \gg |1/T_{1b} - 1/T_{1\mathrm{myo}}|$ and the no (or very slow) water exchange regime, defined as $1/\tau \ll |1/T_{1b} - 1/T_{1\mathrm{myo}}|$, where $1/\tau = 1/\tau_b + 1/\tau_{\mathrm{myo}}$ with τ_b and τ_{myo} being the average residence times of water in the vascular and extravascular compartments, respectively, T_{1b} denotes blood longitudinal relaxation time, and $T_{1\mathrm{myo}}$ denotes myocardial longitudinal relaxation time (2). Second, using a specified MR sequence a two-site exchange model was incorporated into the perfusion model, allowing us to estimate how dependent K_i or F was on the water exchange rate between compartments. In order to validate the predicted results of this model, we performed perfusion measurements using Gd-DTPA in the heart, where Gd-DTPA acts as an extravascular CA, and in the brain, where Gd-DTPA acts as an intravascular CA in normal volunteers (we did not have access to intravascular CA for the heart).

The nomenclature in MR tracer kinetic models is somewhat confusing and in the following we will define transfer constants and concentrations carefully and adhere as

Danish Research Center for Magnetic Resonance, Hvidovre Hospital, University of Copenhagen, Copenhagen, Denmark.

Presented orally at ISMRM, Denver, 2000.

*Correspondence to: Henrik BW Larsson, M.D., Ph.D., Danish Research Center for Magnetic Resonance, Hvidovre University Hospital, Kettegaard Alle 30, DK-2650, Denmark. E-mail: henrikl@magnet.drcmr.dk or hbw.larsson@dadlnet.dk

Received 22 March 2000; revised 22 February 2001; accepted 26 February 2001.

far as possible to the newly proposed standardization of the various terms (18).

MATERIALS AND METHODS

Theory

Following CA administration the intrinsic relaxation rate of each compartment will change. This change is determinated by the tracer kinetic theory giving the concentration of the CA in each compartment for a given set of system parameters such as perfusion, unidirectional transfer constant, volume of distribution, etc. Since the concentration of the CA changes as a function of time the intrinsic relaxation rates will also change (as will also the strict categorization of the system being in a fast or slow water exchange regime). The intrinsic relaxation rates are then passed through a general two-site exchange model with the aim of incorporating the effect of water exchange at all time points during the bolus passage. Solving the differential equations associated with the two-site exchange model (see below) allows one to calculate the magnetization and the MR signal for any MR sequence (in the present study, IR-turboFLASH or SAT-turboFLASH) during the bolus passage in tissue. This was used for simulation of MR signals.

First, tissue concentration curves were generated in the case of $E > 0$, corresponding to an extravascular CA, using one typical input function $C_a(t)$ referring to full blood concentration, obtained in a previous study. In the following we call this the standard input function. The input function can be obtained accurately up to a concentration of 3–4 mM, from the aorta or the left ventricle if *TI* is sufficiently short (<50 ms) (19,20). Longer *TI* results in full relaxation before sampling the MR signal and will therefore result in underestimation of the input function and especially the peak concentration. It should also be noted that water exchange between the red cells and plasma is known to be fast (21). Assuming known values of the influx constant, K_i or, alternately, the transfer constant K^{trans} and the extravascular extracellular volume fraction ν_e ($\equiv V_e/V_t$, i.e., extravascular extracellular volume divided by total tissue volume), the tissue concentration $C_{\text{myo}}(t)$ can be calculated from the Kety equation (13):

$$C_{\text{myo}}(t) = C_p(t)*K^{\text{trans}}\exp\left(-\frac{K^{\text{trans}}}{\nu_e}t\right)$$

$$= C_a(t)*K_i\rho\,\exp\left(-\frac{K_i\rho(1-\text{Hct})}{\nu_e}t\right) \qquad [1]$$

where $C_{\text{myo}}(t)$ (mM) is the number of moles of CA in the extravascular extracellular space divided by the total tissue volume as a function of time. Therefore, $C_{\text{myo}} = \nu_e C_e$, where C_e is the extravascular extracellular concentration. C_p is the plasma concentration of the CA, assuming that the CA does not enter the erythrocytes, and $C_a = C_p(1 - \text{Hct})$. In Eq. [1] we have used the definition $K^{\text{trans}} \equiv K_i\rho(1 - \text{Hct})$ ($= EF\rho(1 - \text{Hct})$)(18). Hct is the small vessel hematocrit, ρ is the density of tissue ($\rho = 1$ g/ml), and * denotes convolution. The residue impulse response function can be represented by a monoexponential function as ($\exp(-K^{\text{trans}}t/\nu_e)$) (see also the Discussion section). By using the expression for the net effective extraction fraction as function of time, $E^{\text{net}}(t) = E(1 - (1 - \text{Hct})C_{\text{myo}}(t)/\nu_e C_a(t))$ (11), the concentration in the vascular space can be approximated to:

$$C_b(t) = (1 - E^{\text{net}}(t))C_a(t)$$

$$= (1 - E)C_a(t) + E\,\frac{1-\text{Hct}}{\nu_e}\,C_{\text{myo}}(t) \qquad [2]$$

where C_b is the tracer concentration in venous whole blood leaving the tissue. By having the vascular and extravascular concentration as a function of time, the intrinsic relaxation rates of the two compartments R_{1b} ($= 1/T_{1b}$) and $R_{1\text{myo}}$ ($= 1/T_{1\text{myo}}$) during the bolus passage of the CA can be calculated as:

$$R_{1\text{myo}}(t) = R_{10\text{myo}} + r_1\,\frac{1}{1-\nu_b}\,C_{\text{myo}}(t) = R_{10\text{myo}} + r_1\,\frac{\nu_e}{1-\nu_b}\,C_e(t)$$

$$R_{1b}(t) = R_{10b} + r_1 C_b(t) \qquad [3]$$

where r_1 is the longitudinal relaxivity. Here, r_1 is assumed to be the same for tissue and blood (22). $R_{10\text{myo}}$ and R_{10b} are the relaxation rates without CA and are equal to 1 s^{-1} and 0.67 s^{-1}, respectively (11). Note $\nu_e + \nu_i + \nu_b = 1$, *where* ν_i is the extravascular intracellular volume divided by total tissue volume and ν_b is the whole blood volume divided by total tissue volume. We assumed fast water exchange between the extravascular extracellular space and extravascular intracellular space (see also the Discussion section).

The MR signal, *SI*, for the two extreme conditions, fast and no-water exchange between the vascular and extravascular space, can be calculated as:

$$SI_{\text{fast}}(t) = SI(\nu_b R_{1b}(t) + (1 - \nu_b)R_{1\text{myo}}(t))$$

$$SI_{\text{no}}(t) = \nu_b SI(R_{1b}(t)) + (1 - \nu_b)SI(R_{1\text{myo}}(t)). \qquad [4]$$

The signal equation for IR-turboFLASH is (23):

$$SI = \Omega M_0 \sin(\alpha)\left(-\frac{\left(C + bA - \frac{1}{\cos(\alpha)}\right)D + 1}{1 + BD}\,e^{-TIR_1}a^{n-1} + (1 - e^{-TIR_1})a^{n-1} + b\,\frac{1-a^{n-1}}{1-a}\right) \qquad [5]$$

where Ω is the receiver gain, M_0 is the fully relaxed magnetization, a is the flip angle, and n is the number of phase encoding steps before reaching $k_y = 0$ (phase encoding direction). *TI* is the time from the center of the 180° RF pulse to the first a pulse, and:

$$a = \cos(\alpha)e^{-TRR_1}$$

$$b = 1 - e^{-TRR_1}$$

$$C = a^{N-1}(1 - e^{-TIR_1})$$

$$A = \frac{1 - a^{N-1}}{1 - a}$$

$$D = \cos(\alpha)e^{-TDR_1}$$

$$B = a^{N-1}e^{-TIR_1}$$

where TR is the repetition time and TD is the time from the last a pulse to the beginning of the next 180° pulse. N is the total number of phase encoding steps for acquiring an image. Equation [5] represents the same signal equation as used in Ref. 11 except that the time between succeeding images has been taken into account. Equation [5] is a steady-state signal expression. The lower of the two equations in Eq. [4] indicates that the expression for the MR signal intensity (Eq. [5]) is used twice, describing the MR signal from the vascular compartment and from the extravascular compartment, respectively, and that the weighted sum of these signals is compatible with a no-exchange situation between these compartments. A disadvantage of the IR-turboFLASH sequence in myocardial studies is that it is sensitive to arrhythmia. Therefore, several studies have used saturation-recovery turboFLASH (SAT-turboFLASH), consisting of an initial nonselective 90° RF pulse followed by FLASH, providing a sequence insensitive to arrhythmia (24). This sequence was also evaluated in this study. The signal equation is:

$$SI = \Omega M_0 \sin(\alpha)\Big((1 - e^{-TIR_1})(\cos(\alpha)e^{-TRR_1})^{n-1} + (1 - e^{-TRR_1})\frac{1 - (\cos(\alpha)e^{-TRR_1})^{n-1}}{1 - \cos(\alpha)e^{-TRR_1}}\Big). \quad [6]$$

The two-site exchange model was implemented in the following way. The water exchange between the vascular and extravascular compartment can be described by two differential equations (25):

$$\frac{dM_b(t)}{dt} = \frac{M_{0b} - M_b(t)}{T_{1b}} - \frac{M_b(t)}{\tau_b} + \frac{M_{\text{myo}}(t)}{\tau_{\text{myo}}}$$

$$\frac{dM_{\text{myo}}(t)}{dt} = \frac{M_{0\text{myo}} - M_{\text{myo}}(t)}{T_{1\text{myo}}} - \frac{M_{\text{myo}}(t)}{\tau_{\text{myo}}} + \frac{M_b(t)}{\tau_b} \quad [7]$$

where τ_{myo} is the water residence time in the extravascular space (i.e., extravascular extracellular space plus extravascular intracellular space, assuming fast exchange between these) and τ_b is the water residence time in the vascular space. Conservation of matter implies $M_{0\text{myo}}/\tau_{\text{myo}} = M_{0b}/\tau_b$ and $M_{0b} + M_{0\text{myo}} = 1$. The solution to these coupled differential equations is:

$$M_b(t) = P_1e^{\psi t} + P_2e^{\varphi t} + M_{0b}$$

$$M_{\text{myo}}(t) = P_3e^{\psi t} + P_4e^{\varphi t} + M_{0\text{myo}} \quad [8]$$

where

$$\psi = -\frac{1}{2}(k_1 + (k_1{}^2 - 4k_2)^{1/2})$$

$$\varphi = -\frac{1}{2}(k_1 - (k_1{}^2 - 4k_2)^{1/2})$$

$$k_1 = \frac{1}{T_{1b}} + \frac{1}{\tau_b} + \frac{1}{T_{1\text{myo}}} + \frac{1}{\tau_{\text{myo}}}$$

$$k_2 = \frac{1}{T_{1b}T_{1\text{myo}}} + \frac{1}{T_{1b}\tau_{\text{myo}}} + \frac{1}{T_{1\text{myo}}\tau_b}.$$

P_1–P_4 are the amplitudes and are dependent on initial conditions. The water exchange process per se is not dependent on the CA bolus passage. However, the initial condition changes following an RF pulse. Therefore, the exchange was implemented in the MR sequence in a forward-step-wise manner. Let i denote the RF excitation number of the single image and j the frame number and let $M(+)$ denote magnetization just after an RF excitation and $M(-)$ magnetization just before RF excitation, then we can write:

$$\begin{bmatrix} M_b(+|t|-)_j^i \\ M_{\text{myo}}(+|t|-)_j^i \end{bmatrix} = \begin{bmatrix} P_{1j}{}^{i-1} & P_{2j}{}^{i-1} \\ P_{3j}{}^{i-1} & P_{4j}{}^{i-1} \end{bmatrix} \begin{bmatrix} e^{\psi t} \\ e^{\varphi t} \end{bmatrix} + \begin{bmatrix} M_{0b} \\ M_{0\text{myo}} \end{bmatrix} \quad [9]$$

reading $M(+|t|-)_j^i$ from left to right as the magnetization as a function of time observed in the time interval after the $(i - 1)$'th pulse to before the i'th pulse of the j'th frame. Taking the following initial condition into account:

$$\begin{bmatrix} M_b(+|t \to 0|-)_j^i \\ M_{\text{myo}}(+|t \to 0|-)_j^i \end{bmatrix} = \begin{bmatrix} M_b(0)_j{}^{i-1}(+) \\ M_{\text{myo}}(0)_j{}^{i-1}(+) \end{bmatrix} = \begin{bmatrix} M_b(0)_j{}^{i-1}(-)\cos(\alpha) \\ M_{\text{myo}}(0)_j{}^{i-1}(-)\cos(\alpha) \end{bmatrix}$$

the amplitude P can be calculated as:

$$P_{1j}{}^{i-1} = \frac{1}{\psi - \varphi}\Big[M_b(0)_j{}^{i-1}(-)\cos(\alpha)\Big(-\frac{1}{T_{1b}(j)} - \frac{1}{\tau_b} - \varphi\Big) + M_{0b}\Big(\frac{1}{T_{1b}(j)} + \varphi\Big) + M_{\text{myo}}(0)_j{}^{i-1}(-)\cos(\alpha)\frac{1}{\tau_{\text{myo}}}\Big]$$

$$P_{2j}{}^{i-1} = -\frac{1}{\psi - \varphi}\Big[M_b(0)_j{}^{i-1}(-)\cos(\alpha)\Big(-\frac{1}{T_{1b}(j)} - \frac{1}{\tau_b} - \psi\Big) + M_{0b}\Big(\frac{1}{T_{1b}(j)} + \psi\Big) + M_{\text{myo}}(0)_j{}^{i-1}(-)\cos(\alpha)\frac{1}{\tau_{\text{myo}}}\Big]$$

$$P_{3j}{}^{i-1} = -\frac{1}{\psi - \varphi}\Big[M_{\text{myo}}(0)_j{}^{i-1}(-)\cos(\alpha) \times \Big(\frac{1}{T_{1\text{myo}}(j)} + \frac{1}{\tau_{\text{myo}}} + \varphi\Big) + M_{0b}\Big(-\frac{1}{T_{1\text{myo}}(j)} - \varphi\Big) - M_b(0)_j{}^{i-1}(-)\cos(\alpha)\frac{1}{\tau_b}\Big]$$

$$P_{4j}^{\,i-1} = \frac{1}{\psi - \varphi}\left[M_{\mathrm{myo}}(0)_j^{\,i-1}(-)\cos(\alpha)\left(\frac{1}{T_{1\mathrm{myo}}(j)} + \frac{1}{\tau_{\mathrm{myo}}} + \psi\right) + M_{0\mathrm{myo}}\left(-\frac{1}{T_{1\mathrm{myo}}(j)} - \psi\right) - M_b(0)_j^{\,i-1}(-)\cos(\alpha)\,\frac{1}{\tau_b}\right].$$

Using these equations, it is possible to calculate the magnetization of each compartment during the entire bolus passage using the IR-turboFLASH or SAT-turboFLASH sequence. $T_{1\mathrm{myo}}(j)$ and $T_{1b}(j)$ take the values corresponding to discretization of Eq. [3] and discretization of the continuous time variable as $t = j \times \delta T$, where δT is the average time between the images of the individual bolus experiment and $j = 1, 2, \ldots, 100$ is the frame number. The flip angle a was set at 180° for IR-turboFLASH and 90° for SAT-turboFLASH, corresponding to the inversion pulse and saturation pulse, respectively, and 15° corresponding to the readout RF pulses. The signal corresponding to the center of k-space, which was reached after 24 readout pulses (asymmetric k-space sampling), was calculated for each frame as:

$$SI(j) = \Omega M_0 \sin(\alpha)(M_b(0)_j^{24}(-) + M_{\mathrm{myo}}(0)_j^{24}(-)) \quad [10]$$

where Ω is the receiver gain and M_0 is the spin density (ΩM_0 is considered as one constant).

For the case where $E = 0$, corresponding to an intravascular CA, the tissue concentration can be calculated as:

$$C_t(t) = C_a(t) * F\rho \exp\left(-\frac{F\rho}{\nu_b}t\right). \quad [11]$$

Note that $C_t(t)$ is the total number of moles in the total tissue volume. The intravascular concentration $C_b(t)$ ($= C_t(t)/\nu_b$) is nearly equal to $C_a(t)$ during the bolus passage (because the CA is confined to the vascular space), but its concentration vs. time profile is broadened slightly by the exponential impulse response function. The concentration of CA in the extravascular space is zero. The intrinsic relaxation rates of two compartments are:

$$R_{1t}(t) = R_{10t}$$

$$R_{1b}(t) = R_{10b} + r_1 C_b(t). \quad [12]$$

R_{10t} is the longitudinal relaxation rate of the tissue without CA. Following the outline as shown for $E > 0$, the two extreme conditions, fast and no-exchange regime, as well as the two-site exchange model could also be simulated for the intravascular CA.

Simulation

A basic prerequisite in tracer kinetic studies is linearity between the input and output of a system. In the present context, this means a linear relation between the input function, $C_a(t)$, and the $R_1(t)$ of the tissue. It is expected that water exchange between compartments can result in a nonlinear relationship. This was investigated by simulation by taking the standard input function, $C_a(t)$, and multiplying this by 3, 5, 7, 9, 11, 13, 15 (see Fig. 1). $C_a(t) \times$ 15 reaches a peak concentration of 25 mM. The two-site exchange model and the IR-turboFLASH sequence with short *TI* (20 ms) were used to generate signal curves for all the input functions, considering both $E = 0$ and $E = 50\%$. In all cases $\tau_b = \frac{1}{3}$ s, a realistic value taken from the literature (2), resulting in a slow water exchange regime. Equation [5] was used to convert the signal curves to R_1 curves.

K_i and F were found from these signal curves using the exponential kernel $\exp(-(1 - \mathrm{Hct})K_i\rho t/\nu_e)$ and $\exp(-F\rho t/\nu_b)$, respectively, using standard fitting procedures (9,11). This method of calculating K_i and F ignores the effect of water exchange. Further, this simulation cannot be validated experimentally in humans because of the very high concentration of Gd-DTPA. Consequently, we performed the following simulation, which could be validated in humans experimentally.

Signal curves were generated using the standard input function and IR-turboFLASH for the two extreme situations, fast and no-exchange regime (Eq. [4]) and also the slow-exchange regime with $\tau_b = \frac{1}{3}$ s (two-site model) for different combinations of *TI* and *E*. This was carried out twice, either with F set to 100 or 500 ml/100 g/min. The high value of F was chosen in order to illustrate the situation in the heart during maximal perfusion, such as after administration of dipyridamole.

Next, the standard input function $C_a(t)$ multiplied by 15 was used to generate fast, no-exchange, and slow-exchange ($\tau_b = \frac{1}{3}$ s) signal curves for short *TI* (= 20 msec) and different values of *E*. In this case, both the IR-turboFLASH and the SAT-turboFLASH sequences were used with the aim of investigating the sensitivity of the MR sequence parameters to water exchange. In all these simulations, ν_b was 10% and ν_e was 20%, and F was set to 100 ml/100 g/min.

Finally, perfusion F was estimated from simulated MR signal enhancement curves generated by the two-site exchange model with $E = 0$, simulating an intravascular CA such as Gd-DTPA in the brain. The simulated curves were generated for the IR-turboFLASH sequence and in all cases with perfusion $F = 60$ ml/100 g/min, $\nu_b = 6\%$, τ_b in the range from 0.003–33 s and *TI* from 20 ms to 1 s. Perfusion F was then estimated simply by relating the simulated MR signal curves to R_1, using Eq. [5], and then estimate F from Eq. [11]. This method of estimating the perfusion corresponds to completely ignoring water exchange between the vascular and the extravascular space in the brain. The standard input function was used both for generating curves and for estimating the perfusion F.

Experimental Procedure

Linearity in perfusion studies between input and output cannot be tested in humans by using very high concentration of CA. But it has been shown that the initial slope of the relaxation curve with *TI* is independent of the water exchange rate (25), and therefore a fast and no-exchange model should not depend on the exchange rate even if a CA is present (4,5). However, we assume that the effect of slow water exchange will be revealed if a longer *TI* is used. Therefore, we used an IR-turboFLASH sequence, consisting of a nonselective 180° RF-pulse, followed by imaging

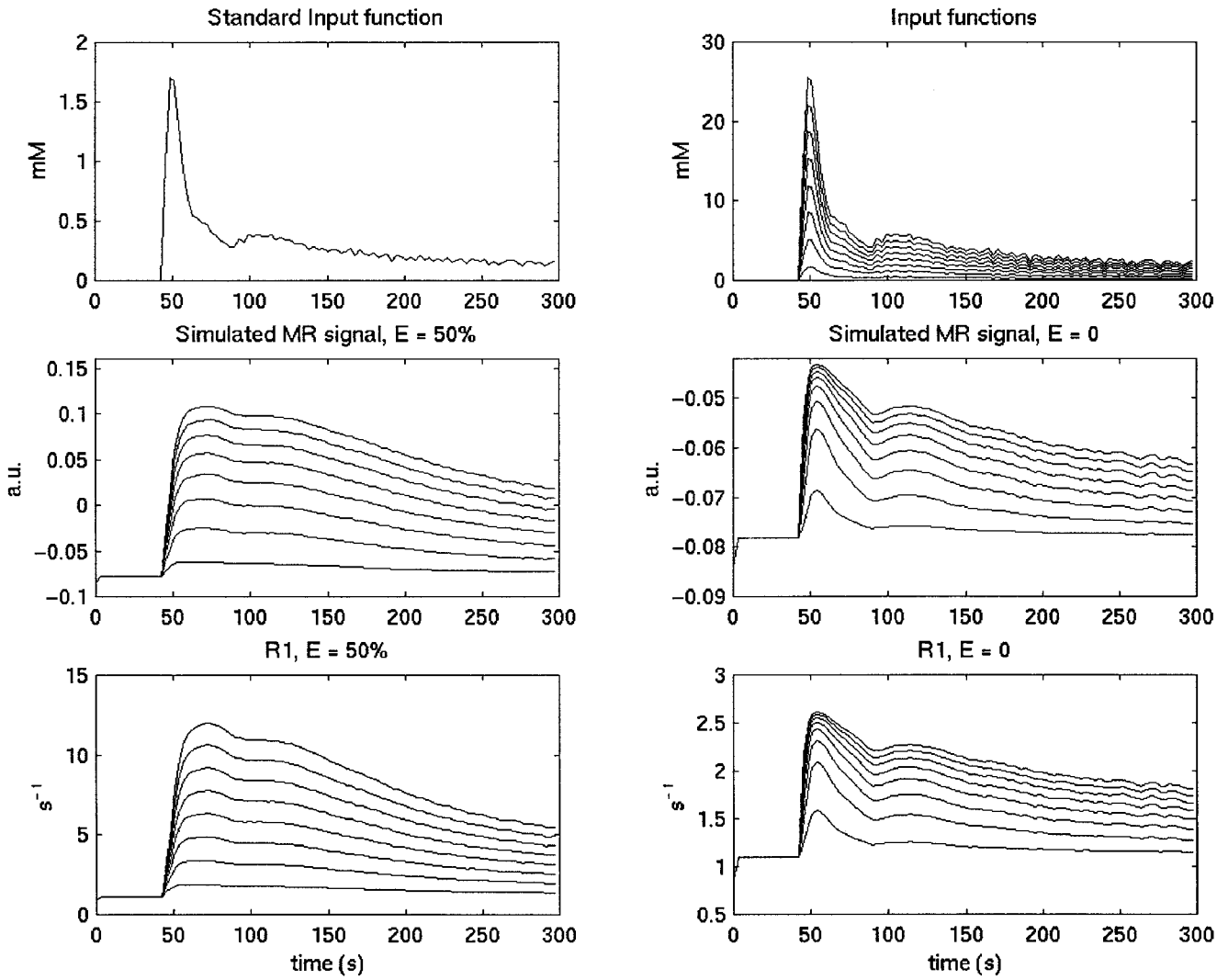

FIG. 1. Upper left: standard input function. Upper right: standard input function multiplied by 3, 5, 7, 9, 11, 13, 15. Middle left: tissue signal curves generated by the two-site exchange model for $E = 50\%$ for the various input functions. Middle right: as before but $E = 0\%$. Lower left: R_1 estimated from the signal curves where $E = 50\%$, using relevant signal expression. Lower right: R_1 estimated from the signal curves where $E = 0\%$, using relevant signal expression. In all cases, F was set to 100 ml/100 g/min, the vascular space 10%, interstitial space 20%, and $\tau_b = 0.3$ s.

of two slices obtained with a short and a long *TI*. It is hypothesized that if similar results are obtained with short and long *TI* the water exchange regime will not have any impact on K_i or F.

The study was performed on a Vision Magneton (Siemens) at 1.5 T. The heart was investigated in seven healthy subjects and the brain in six. On the basis of the scout images of the heart, two slices were placed transaxially with the slice with the short *TI* placed closer to the base of the heart than the slice with the long *TI*. Both slices covered representative areas of the septum and the anterior wall. The input function was always calculated from the slice with the short *TI*. In the brain, the slices were also placed transaxially, with one slice placed at the level of the Circle of Willis, covering major intracerebral arteries, and the other slice placed at the level of the basal ganglia. The input function was calculated from the slice with the short *TI* from the signal in the internal carotid or the anterior cerebral artery. Both slices showed representative areas of gray matter. Before CA injection, T_1 was measured in both slices using the IR-turboFLASH sequence with increasing *TI* (20, 50, 100, 150, 200, 300, 400, 500, 800, 1000, 1500, 3000 ms) as described in a previous study (11). In all cases, the slice thickness was 8 mm, matrix 92×128 (with asymmetric phase encoding reaching k_y zero after 24 steps), $TR/TE = 4/2$ ms, flip angle = 15°. Field of view was 0.3 m in the heart and 0.23 m in the brain. The bolus passage was followed by 100 consecutive sets (two slices) of IR-turboFLASH images with a time resolution of 3 s; in the heart the sequence was triggered on every third heartbeat. The CA was injected via a superficial vein using a power injector (0.1 mmol/kg ~ 0.2 ml/kg, speed 3 ml/s) after having acquired the first 10 sets of images, which were used as the baseline for calibration (11). The short *TI* was 20 ms for heart and brain and the long *TI* was 550–693 ms (dependent on the heart rate) for the heart and

Table 1
Calculation of K_i and F From Simulated Data Corresponding to Fig. 1

C_a	× 1	× 3	× 5	× 7	× 9	× 11	× 13	× 15
K_i^*	54	52	51	54	48	52	52	49
F^*	95	46	26	17	13	9	7	6

*ml/100 g/min.

600–1000 ms for the brain during the bolus passage. Regions of interest (ROIs) were placed in the left ventricle (10–25 pixels), in the septum and the anterior myocardial wall (10–20 pixels), and in occipital gray matter (5–15 pixels). The position of the ROI in the arteries in the brain was carefully placed using the time frame where the major arteries were most clearly seen, typically at the bolus peak, and the ROIs contained only 2–4 pixels. Signals were read out from these ROIs and data evaluated by relating the MR signal to R_1, using Eq. [5] where ΩM_0 is found from the baseline images (before appearance of Gd-DTPA) and the initial T_1 measurement and then estimating K_i (heart) and F (brain) from Eqs. [1] and [11], respectively (9,11). It should be pointed out that this calculation completely ignores the effect of water exchange between compartments. As all subjects were healthy and without MR-visible lesions, the unidirectional influx constant, K_i, and the perfusion, F, were assumed to be similar for both slices, i.e., for short and long *TI*. The protocols were approved by the local ethics committee.

RESULTS

Simulation

Figure 1 shows the standard input function and the standard input function multiplied by the factors 3, 5, 7, 9, 11, 13, 15. The last input function therefore reaches a peak concentration of 25 mM. This concentration is unrealistic in humans but has been used in simulation studies previously. The figure also shows simulated tissue signal curves for all the input functions, using the two-site exchange model ($\tau_b = \frac{1}{3}$ s, $\tau_{myo} = 3$ s) in the case of $E = 50\%$ and $E = 0\%$. *TI* was short (20 ms). The estimated R_1 for the tissue for the various input functions is also shown for both $E = 50\%$ and $E = 0\%$. Clearly the system is not linear in the case of $E = 0\%$ but seems reasonably linear in the case of $E = 50\%$. This is supported by calculating K_i and the perfusion F for the various input functions and tissue signal curves, as shown in Table 1. As can be seen, K_i is unaffected regardless of the input function used, whereas the perfusion, F, decreases when higher input functions are used.

Figure 2 shows fast, no-exchange, and slow-exchange tissue signal enhancement curves using the standard input function and F set to 100 ml/100 g/min (simulating a rest condition) for various combinations of E and *TI*. Clearly the three conditions, fast, no exchange, and slow exchange, do not differ greatly for $E > 30\%$ regardless of *TI*. However, a separation of the curves for the three exchange conditions is seen for $E \leq 20\%$ and higher values of *TI* (above 20 ms). Importantly, this pattern was not changed by setting F to 500 ml/100 g/min, corresponding to a stress situation.

Figure 3 shows tissue signal curves for the three exchange conditions using the standard input function × 15 for short *TI* (20 ms) and different values of E. Both IR-turboFLASH and SAT-turboFLASH are considered. It is apparent that the inversion recovery and saturation recovery sequence are very similar with regard to sensitivity to water exchange. There is also a clear difference between fast and slow exchange for $E \leq 30\%$. This becomes very pronounced when $E = 0\%$.

Figure 4 shows the results of calculation of the perfusion F, for various combinations of τ_b and *TI*, for $E = 0$. When the water exchange rate between compartments is not fast, it is clearly seen that the two-site exchange model predicts much lower perfusion values for longer values of *TI*.

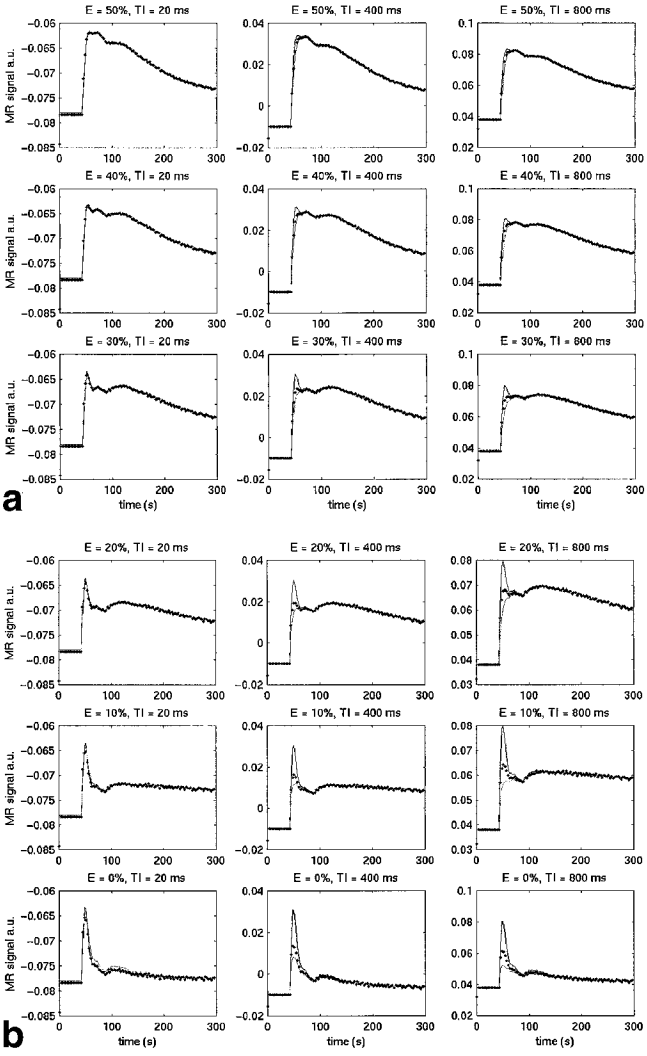

FIG. 2. **a,b:** MR signal enhancement curves for fast, slow, and no-exchange conditions for various combinations of extraction fraction (*E*) and *TI* using the standard input function. In all cases, *F* was set to 100 ml/100 g/min, the vascular space was 10%, interstitial space 20%. When the three curves are seen separately, the highest curve always represent fast exchange, followed by the intermediate/slow exchange (dots), with vascular water residence time of $\frac{1}{3}$ sec, and then the no-exchange curve. Note that the separation primarily occurs around the peak concentration.

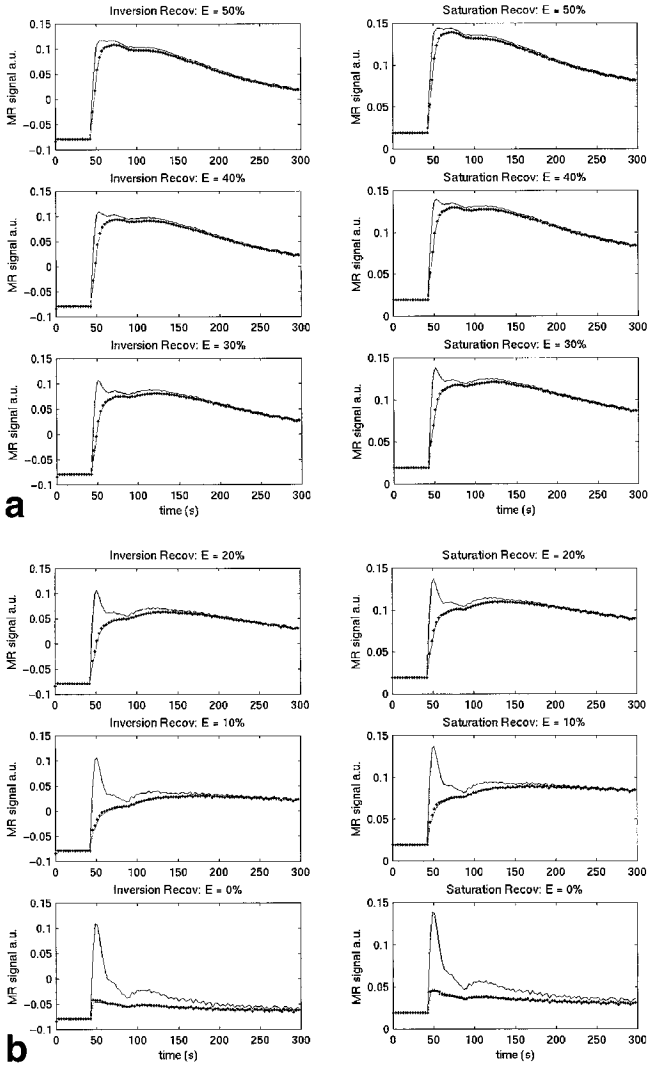

FIG. 3. **a,b:** MR signal enhancement curves for fast, slow ($\tau_b = 0.3$ sec), and no-exchange conditions for various extraction fractions (*E*), keeping *TI* short (20 ms), using the standard input function × 15. In all cases, *F* was set to 100 ml/100 g/min, the vascular space was 10%, and the interstitial space 20%. The left column shows conditions when using IR-turboFLASH and the right column when using saturation recovery turboFLASH. Note that for this high input function the curves stay separate even after bolus peak for $E = 0\%$, and that a *TI* of 20 ms is too long to compensate for water exchange.

In Vivo Results

K_i for the myocardium was 64.5 ± 13.2 (mean ± SD) ml/100 g/min for short *TI*, and 58.7 ± 18.9 ml/100 g/min for long *TI* ($P > 0.05$ using Wilcoxon's rank sum test for paired observations).

The perfusion, *F*, in gray matter was 80 ± 15 ml/100 g/min for short *TI* and significantly lower for long *TI* (see Fig. 4). The difference between *F* obtained with short and long *TI* was significant ($P < 0.001$, Wilcoxon's test for paired observations).

Figure 5a,b shows tissue enhancement curves for ROIs placed in the myocardial septum obtained with short and long *TI*. The curves in Fig. 5a,b are obtained from the same subject. Note that the signal increase is higher for the longer *TI* than the shorter *TI*, as would be expected for a simple system not complicated by the water exchange. Figure 5c,d shows tissue enhancement curves for ROIs placed in occipital grey matter and obtained with short and long *TI*. Note that the signal increase is of comparable size for short and long *TI*, indicating some damping of the system at long *TI*. The simulation predicts this effect to be due to a nonfast water exchange. The models represented by Eqs. [1] and [11] are fitted to the myocardial and brain signal enhancement curves, respectively, and are shown as fully drawn curves in Fig. 5. As shown, even though the model represented by Eq. [11] fits the two brain curves obtained with short and long *TI* equally well, the estimated perfusion when obtained with the long *TI* is much lower than when obtained with the short *TI*.

DISCUSSION

An important finding of this study is that the water exchange between the vascular and the extravascular extracellular space does not have any effect on the determination of the myocardial perfusion marker, the unidirectional influx constant K_i, or, alternatively the volume transfer constant K^{trans} for CA diffusion over the capillary membrane, if a realistic dose is used and if a realistic extraction fraction, *E*, of the CA is considered. This is shown both theoretically and experimentally. An intravenous dose of 0.1 mmol/kg of Gd-DTPA will not give a higher input function in humans than the standard input function used in the present study for the simulation (20). An extraction fraction of 40–50% for Gd-DTPA is very likely during resting conditions (26). However, in Ref. 26 an increase of the extraction fraction was found for de-

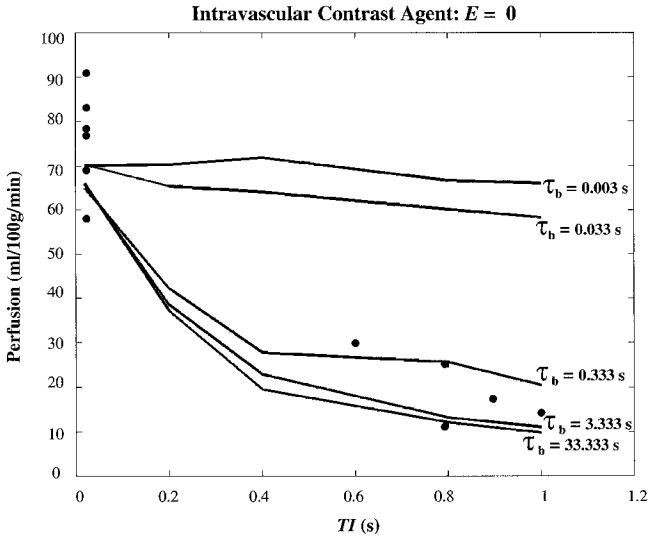

FIG. 4. Calculated perfusion (*F*) (lines) from simulated signal enhancement curves generated from the two-site exchange model for $E = 0$ (simulating an intravascular CA) for various combinations of *TI* and τ_b. In the simulation, *F* was set to 60 ml/100 g/min and v_b was 6%. Dots represent actual measured perfusion of gray matter of healthy volunteers at different values of *TI* when using inversion recovery Turbo-FLASH and Gd-DTPA.

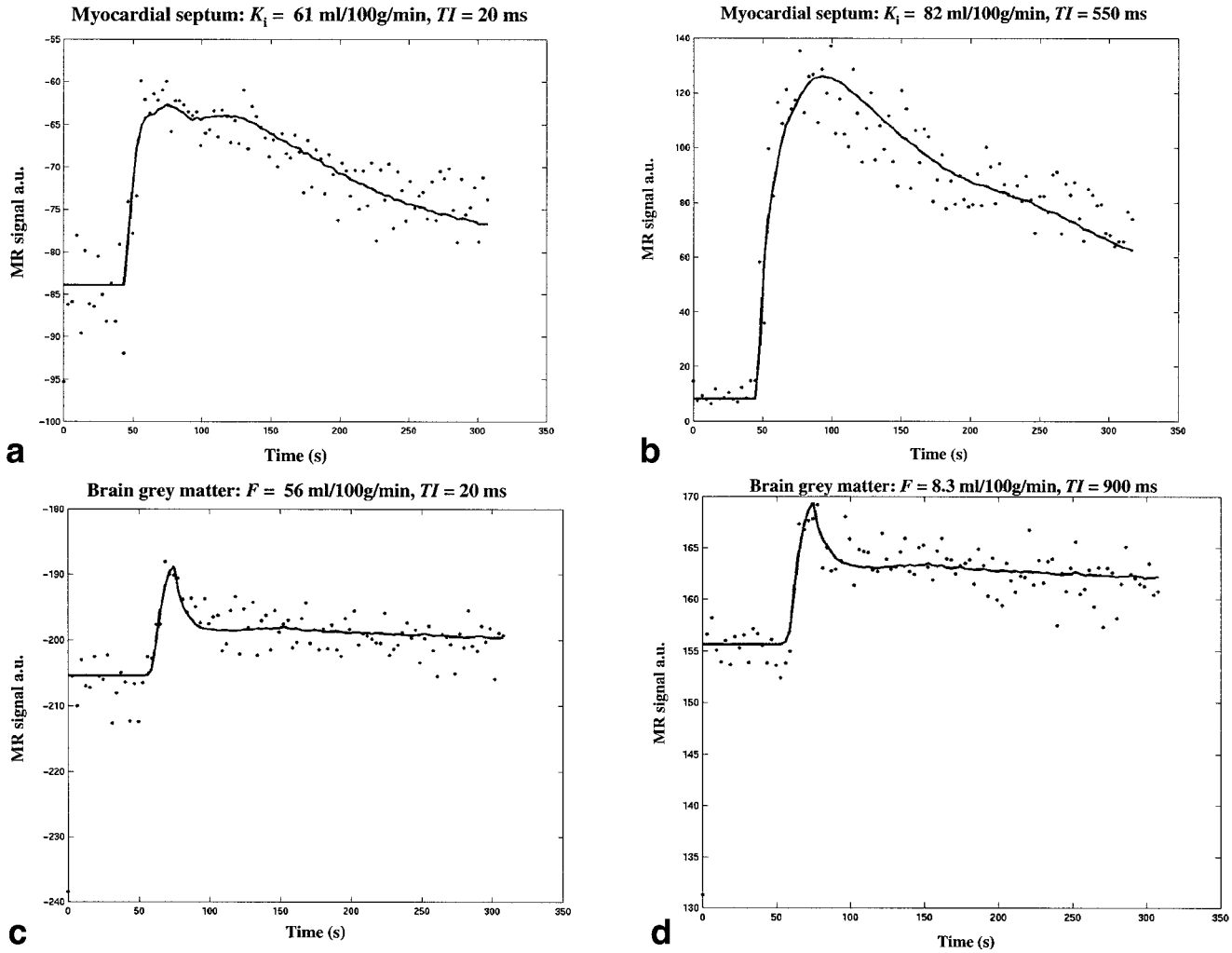

FIG. 5. **a,b,c,d:** Myocardial and brain example. **a:** Myocardial enhancement curve from an ROI placed in the myocardial septum (23 pixels) obtained with short *TI*. The fully drawn curve is the model, represented by Eq. [1], fitted to data. **b:** Myocardial enhancement curve from the same subject as in **a**. ROI was placed in the septum (15 pixels) and *TI* was long. **c:** Enhancement curve from an occipital gray matter ROI (9 pixels) obtained with short *TI*. Fully drawn curve represents the model fit (represented by Eq. [11]) to data. **d:** Enhancement curve from the same subject as in **c.** ROI (14 pixels) was placed in occipital gray matter and *TI* was long.

creasing perfusion in canine myocardium (the extraction fraction was sometimes above unity, indicating some methodological problems in the measurements), but the extraction fraction appeared rather constant for perfusion in the range of 40–140 ml/100 g/min. The finding of a perfusion reserve index (K_i stress/K_i rest) of 2–4 in humans (16,17) is not in agreement with a significant lowering of the extraction fraction when perfusion is increased above 200–300 ml/100 g/min. We also simulated a stress condition such as that created by infusion of dipyridamole, which is known to result in vascular vasodilatation in the heart. Setting F to 500 ml/100 g/min did not change Fig. 2. Separation of the three curves was again only seen for an extraction fraction below 30% and for *TI* above 20 ms. Ongoing in vivo studies are trying to verify this prediction.

Another important finding is that total exclusion of the CA from a compartment, corresponding to $E = 0$, seems to facilitate separation of enhancement curves corresponding to fast, intermediate/slow, and no water exchange, and this finding is not dependent on the type of MR sequence used for monitoring the enhancement. However, for the extraction fraction approaching zero, K_i or perfusion F can be determined correctly if sequence timing is kept short (and the dose of CA is not too large). This is in accord with Hazlewood et al. (25), who showed that the initial slope of the relaxation curve is independent of relaxation rate. The present methodology provides quantitative information on the effect of water exchange on the determined values of K_i and F.

The presented model predicts that nonlinearity between input function and tissue response, in this case ΔR_1, will occur for increasing *TI*. This is an advantage, as linearity cannot be assessed by increasing the dose in human studies. In addition, a T_2^* effect would have to be considered at high concentrations of CA.

Several studies have considered water exchange between the vascular and extravascular space and between

the extravascular extracellular and extravascular intracellular space. The study of Wendland et al. (3) points to a slow water exchange rate between the vascular and interstitial space (extravascular extracellular space), or between interstitial and extravascular intracellular space when extravascular CA is used. The exact concentration range in this study is difficult to estimate, as only the dose of CA was reported and the time resolution of imaging relative to heart rate was poor. They used a very long *TI* (700 ms) and assessment of the linearity of the system was based on the signal increase being in proportion to the dose. As seen from Fig. 1, ΔR_1 can be linear with the concentration, while the signal is not necessarily so. In the study of Donahue et al. (2), the exchange regime was investigated in rat and frog heart ex vivo using Gd-DTPA and Gd-DTPA-BSA. Under these steady-state conditions, the exchange rate could be determined by simulation. The vascular–extravascular exchange rate was estimated to be 1–6 s^{-1}, indicating slow exchange, and the extravascular extracellular–intracellular exchange rate to be 8–27 s^{-1}, indicating fast exchange. In another very comprehensive study by Donahue et al. (5), intravascular CA was used to measure the size of the vascular space under steady-state conditions. The results showed the estimated vascular space to be very dependent on the model used (fast or no-exchange model), timing of MR sequence (*TI* or *TR*), concentration range of CA, and water exchange rate between compartments. By simulation it was shown that if *TI* (or *TR*) was kept short, accurate measures of the vascular space could be obtained. The present study shows that this concept is also applicable to perfusion studies. As shown, the accuracy of the perfusion *F* can be increased by keeping *TI* short. Using a two-site water exchange model different from ours, Judd et al. (6) concluded that the slow water exchange between vascular and extravascular extracellular space had a significant impact on the estimation of perfusion when using either intravascular or extravascular CA. In particular, they observed that when using an input function with peak concentration of about 25 mM and a first pass extraction fraction of 15–30%, R_1 was not linear with the concentration of the input function. While our results are in complete accord with this (see Fig. 3, which shows significant differences between fast and no-water exchange for *E* between 10–30%) we do not agree with their general conclusion about extracellular CA. In fact, their figure 2 shows experimental evidence for linearity between realistic input functions and tissue R_1 changes. It should also be noted that it is not the peak R_1 which reflects K_i or perfusion *F* but the initial slope of the enhancement curve.

Other studies have utilized the steady-state conditions by equalizing the vascular and interstitial space with extravascular CA. Under these conditions high transient concentrations of intravascular CA do not occur and can be ignored. In a study by Wedeking et al. (1), it was found that R_1 was linear in myocardium and skeletal muscle in the range of 0–0.6 μmol/g (GdHP-DO3A), and in the study of Donahue et al. (2), R_1 was linear with Gd-DTPA up to 2 mM. It should be mentioned that the use of the standard input function and *F* of about 100 ml/100 g/min and *E* of about 50% never results in tissue concentrations over 0.5 mM (approximately 0.3 mM for a dose of 0.1 mmol/kg, a vascular space of 10% and interstitial space of 20%), and we assume that this is the reason for not finding any difference in K_i for long and short *TI* in this study. Recently, in a study by Landis et al. (27) linearity was found only for a tissue concentration of ≤0.1 mM Gd-DTPA in skeletal muscle. This was taken as an indication of a much slower water exchange rate between extravascular extracellular space and extravascular intracellular space than is generally thought. We believed that such an effect of slow water exchange between these compartments would have shown up in our myocardial data for long *TI*, if present. On the other hand, a subtle effect of increasing *TI* on K_i could have been masked because of the uncertainty of the estimated K_i, and the use of even longer *TI* may reveal this effect, if present. Therefore, additional simulations and validation studies seem necessary.

Fast and no-exchange tissue enhancement signal curves are almost identical for a clinically relevant dose of CA and reasonable values of K_i and *E*, etc., and therefore it could be expected that K_i would approach the perfusion, *F*, of the heart, which is about twice the value of K_i. The reason this does not happen is that, even for really fast water exchange between the vascular and extravascular compartments, the system is still a two-compartment system and the use of a monoexponential kernel for deconvolution would extract a value of about the real K_i and not *F*, as can be shown by simulation. In fact, there is some uncertainty about what kind of analytical residue impulse function should be used for the deconvolution, but no detailed comparison between different functions exists. In this study, we used a monoexponential function as residue impulse response function. A Fermi function has been suggested previously (11) and partially validated (28) in myocardial perfusion imaging. Our preliminary results do not show any improvement in the goodness of the fit from the use of a Fermi function instead of a monoexponential function, and a Fermi function results in the same values of K_i as a monoexponential function. However, our preliminary results show that singular value decomposition (SVD) gives higher values of K_i, possibly reflecting its ability to detect multiple subsystems (data not shown).

The result of the application of the IR-turboFLASH for brain perfusion measurement has only been presented in abstract form previously (29). One advantage of this method is that it monitors concentration by T_1 changes, and that the relation between concentration and T_1 change is not affected by susceptibility, vessel geometry, and distance between vessels as T_2^* changes are, so the relaxivity is more reliable. Another advantage is that input functions are readily obtained in contrast to input functions obtained with T_2^*-weighted sequences. The disadvantage is the poor SNR for the tissue signal enhancement, especially for short *TI*, and of course the impact of water exchange. However, the last factor may be an advantage in that the water residence time could be incorporated into the perfusion model and therefore be estimated together with the perfusion. The results could also have implications for the arterial spin-labeling technique and one could anticipate a similar relationship between perfusion determined by arterial spin-labeling and *TI* when using exogeneous CA, as in the present study.

CONCLUSION

Water exchange between vascular and extravascular extracellular space will not have any effect on the determination of K_i for a realistic dose of CA and an extraction fraction above 30%, even for *TI* up to nearly a second. This also implies that multislice myocardial perfusion imaging is possible and up to at least five slices can now be covered in one cardiac cycle. Intravascular CA will be much more affected by the water exchange between the vascular and extravascular compartments and extracted physiological parameters will be dependent on compartment size, MR sequence timing, and the water residence time. However, if *TI* is kept short estimation of the perfusion is not seriously affected by water exchange. Finally, Eqs. [7] to [10] used in the simulation can also be used in fitting experimentally obtained data, representing a new method of estimating K_i or F and possibly also water residence time in different compartments. This method also eliminates the sensitivity of IR-turboFLASH to arrhythmia if the exact time for obtaining the images during the bolus passage is sampled. This variable timing can easily be incorporated into the equations. In addition, the rate of obtaining images can easily be increased above one image per 3 sec, because Eqs. [7]–[10] do not rely on a steady-state condition as Eq. [5]. Consequently, the advantages of IR-turboFLASH over SAT-turboFLASH can now be used to its full extent providing a larger signal range and increased SNR when using a higher CA dose. This will increase the accuracy of estimates derived from dynamic contrast MRI measurements in tissues such as the heart and brain.

REFERENCES

1. Wedeking P, Sotak CH, Telser J, Kumar K, Chang CA, Tweedle MF. Quantitative dependence of MR signal intensity on tissue concentration of Gd(HP-DO3A) in the nephrectomized rat. Magn Reson Imag 1992;10:97–108.
2. Donahue KM, Burstein D, Manning WJ, Gray ML. Studies of Gd-DTPA relaxivity and proton exchange rates in tissue. Magn Reson Med 1994; 32:66–76.
3. Wendland MF, Saeed M, Yu KK, Roberts PL, Lauerma K, Derugin N, Varadarajan J, Watson AD, Higgins CB. Inversion recovery EPI of bolus transit in rat myocardium using intravascular and extravascular gadolinium-based MR contrast media: dose effects on peak signal enhancement. Magn Reson Med 1994;32:319–329.
4. Schwickert HC, Roberts TPL, Shames DM, van Dijke CF, Disston A, Muhler A, Mann JS, Brasch RC. Quantification of lever blood volume: comparison of ultra short TI inversion recovery echo planar imaging (ULSTIR-EPI), with dynamic 3D-gradient recalled echo imaging. Magn Reson Med 1995;34:845–852.
5. Donahue KM, Weisskoff RM, Chesler DA, Kwong KK, Bogdanov AA, Mandeville JB, Rosen BR. Improving MR quantification of regional blood volume with intravascular T_1 contrast agents: accuracy, precision, and water exchange. Magn Reson Med 1996;36:858–867.
6. Judd RM, Reeder SB, May-Newman K. Effects of water exchange on the measurement of myocardial perfusion using paramagnetic contrast agents. Magn Reson Med 1999;41:334–342.
7. Diesbourg LD, Pratto FS, Wisenberg G, Drost DJ, Marshall TP, Carroll SE, O'Neill B. Quantification of myocardial blood flow and extracellular volume using a bolus injection of Gd-DTPA: kinetic modeling in canine ischemic disease. Magn Reson Med 1992;23:238–253.
8. Wilke N, Simm C, Zhang J, Ellermann J, Ya X, Merkle H, Path G, Ludemann H, Bache RJ, Ugurbil K. Contrast-enhanced first pass myocardial perfusion imaging: correlation between myocardial blood flow in dogs at rest and during hyperemia. Magn Reson Med 1993;29:485–497.
9. Larsson HBW, Stubgaard M, Sondergaard L, Henriksen O. In vivo quantification of the unidirectional influx constant for Gd-DTPA diffusion across the myocardial capillaries with MR imaging. J Magn Reson Imag 1994;4:433–440.
10. Wilke N, Kroll K, Merkle H, Wang Y, Ishibashi Y, Xu Y, Zhang J, Jerosch-Herold M, Muhler A, Stillman AE, Bassingthwaighte JB, Bache R, Ugurbil K. Regional myocardial blood volume and flow: first-pass MR imaging with polylysine-Gd-DTPA. J Magn Reson Imag 1995;5: 227–237.
11. Larsson HBW, Fritz-Hansen T, Rostrup E, Søndergaard L, Ring P, Henriksen O. Myocardial perfusion modeling using MRI. Magn Reson Med 1996;35:716–726.
12. Vallée JP, Sostman HD, MacFall JR, Wheeler T, Hedlund LW, Spritzer CE, Coleman RE. MRI quantitative myocardial perfusion with compartmental analysis: rest and stress study. Magn Reson Med 1997;38:981–989.
13. Kety SS. The theory and application of the exchange of inert gas in lung and tissues. Pharmacol Rev 1951;3:1–41.
14. Fenstermacher JD, Blasberg RG, Patlak CS. Methods for quantifying the transport of drugs across brain barrier systems. Pharm Ther 1981;14: 217–248.
15. Vallée JPM, Sostman HD, MacFall JR, DeGrado TR, Zhang J, Sebbag L, Cobb FR, Wheeler T, Hedlund LW, Turkington TG, Spritzer CE, Coleman E. Quantification of myocardial perfusion by MRI after coronary occlusion. Magn Reson Med 1998;40:287–297.
16. Fritz-Hansen T, Rostrup E, Søndergaard L, Ring P, Amtorp O, Larsson HBW. Capillary transfer constant of Gd-DTPA in the myocardium at rest and during vasodilation assessed by MRI. Magn Reson Med 1998; 40:922–929.
17. Cullen JHS, Horsfield MA, Reek CR, Cherryman GR, Barnett DB, Samani NJ. A myocardial perfusion reserve index in humans using first-pass contrast-enhanced magnetic resonance imaging. J Am Coll Cardiol 1999;33:1386–1394.
18. Tofts PS, Brix G, Buckley DL, Evelhoch JL, Henderson E, Knopp MV, Larsson HBW, Lee TY, Mayr NA, Parker GJM, Port RE, Taylor J, Weisskoff RM. Estimating kinetic parameters from dynamic contrast-enhanced T_1-weighted MRI of a diffusable tracer: standardized quantities and symbols. J Magn Reson Imag 1999;10:223–232.
19. Fritz-Hansen T, Rostrup E, Ring PB, Larsson HB. Quantification of gadolinium-DTPA concentrations for different inversion times using an IR-Turbo FLASH pulse sequence: a study on optimizing multisclice perfusion imaging. Magn Reson Imag 1998;16:893–899.
20. Fritz-Hansen T, Rostrup E, Larsson HBW, Søndergaard L, Ring P, Henriksen O. Quantification of the input function using MRI. A step towards quantitative perfusion imaging. Magn Reson Med 1996;36: 225–231.
21. Koenig SH, Spiller M, Brown RD, Wolf GL. Relaxation of water protons in the intra- and extracellular regions of blood containing Gd(DTPA). Magn Reson Med 1986;3:791–795.
22. Pereira RS, Prato FS, Sykes JM, Wisenberg G. Assessment of myocardial viability using MRI during a constant infusion of Gd-DTPA: further studies at early and late periods of reperfusion. Magn Reson Med 1999;42:60–68.
23. Brix G, Schad LR, Deimling M, Lorenz WJ. Fast and precise T1 imaging using a tomrop sequence. Magn Reson Imag 1990;8:351–356.
24. Tsekos N, Zhang Y, Merkle H, Wilke N, Jerosch-Herold M, Stillman AE, Ugurbil K. Fast anatomical imaging of the heart and assessment of myocardial perfusion with arrythmia insensitive magnetization preparation. Magn Reson Med 1995;34:530–536.
25. Hazlewood C, Chang D, Nichols B, Woessner D. Nuclear magnetic resonance transverse relaxation times of water protons in skeletal muscle. Biophys J 1974;14:583–605.
26. Tong CY, Prato FS, Wisenberg G, Lee TY, Carroll E, Sandler D, Wills J, Drost D. Measurement of the extraction efficiency and distribution volume for Gd-DTPA in normal and diseased canine myocardium. Magn Reson Med 1993;30:337–346.
27. Landis CS, Li X, Telang FW, Molina PE, Palyka I, Vetek G, Springer CS. Equilibrium transcytolemmal water-exchange kinetics in skeletal muscle in vivo. Magn Reson Med 1999;42:467–478.
28. Jerosch-Herold M, Wilke N, Stillman A. Magnetic resonance quantification of the myocardial perfusion reserve with a Fermi function model for constrained deconvolution. Med Phys 1998;25:73–84.
29. Larsson HBW, Rosenbaum S, Rostrup E, Fritz-Hansen T. Quantification of the brain perfusion using Gd-DTPA and T_1 measurements. In: Proc ISMRM 7th Annual Meeting, Philadelphia, 1999. p 1864.